DOI: 10.15480/882.9369

Eighth International Symposium on Marine Propulsors
smp'24, Berlim, Germany, March 2024

# Magnetic based current turbine

**João Victor Padilha de Lima**[1,2], **Antonio Carlos Fernandes**[1], **Moustafa Abdel-Maksoud**[2]

[1]Federal University of Rio de Janeiro, Rio de Janeiro, Brazil
[2]Institute for Fluid Dynamics and Ship Theory, Hamburg University of Technology, Hamburg, Germany

**ABSTRACT**
This paper presents the concept of an innovative current turbine based on magnetic restoration and optimizes its design. The evaluation of the turbine's geometries and power take-off mechanism is carried out based on the numerical solution of a non-linear mathematical model already experimentally validated for the proposed system and considers a realistic operational condition. The parameter to be optimized is the turbine operating efficiency. The parameters are optimized within smaller ranges to reach a local optimum within the design space. The reduction of parameter ranges is based on the results of the best turbine configurations.

**Keywords**
Turbine optimization, Current turbine, Magnetic restoration, Parametric model, Non-linear system

## 1 INTRODUCTION

Recent international agreements, such as the Paris Agreement (ONU 2015), the European Green Deal (EU 2019), and the Kyoto Protocol (ONU 1998), reflect global efforts to reduce dependence on fossil fuels. The commitment to decrease greenhouse gas emissions by 55% by 2030, as outlined in the Kyoto Protocol, underscores the urgency to address the challenges associated with fossil fuel consumption. These challenges include supply constraints and environmental concerns, prompting the exploration of cleaner and renewable energy sources (Rahman et al. 2022). Notably, solar incidence, wind, and water movement (including rivers, tides, and ocean currents) are the focal points of numerous initiatives in the quest for sustainable energy (Elavarasan 2019).

This article specifically delves into various methods of harnessing energy from moving water, focusing on the limitations of conventional water turbines like Francis (Yasuyuki et al. 2004), Propeller (Hood 1910), Kaplan (Sproule 1961), and Pelton (Erlach 1889) turbines, commonly employed in large-scale hydroelectric power plants. The primary drawback of these turbines lies in their reliance on substantial waterfalls, often necessitating the construction of dams and reservoirs, which are both costly and environmentally problematic (Bagher et al. 2015), (Zhou et al. 2013)) and (Loney 1995).

Recognizing the drawbacks associated with dam construction, this study advocates for harnessing hydroelectric power from minor waterfalls without the need for dams. This approach not only presents a renewable solution but also minimizes environmental impact, avoiding issues like wildlife disruption and sediment accumulation (Dametew 2016).

The Axial Flow Rotor (Noel 1967), Open Center Fan (Williams 2006), and Helical turbines (Naskali et al. 2005) emerge as the frequently employed hydroelectric turbines for minor waterfalls. However, structural flaws induced by centrifugal stress in these designs necessitate high-performance materials, prompting a search for alternative turbine movements with reduced stress (Peng and Zhu 2009).

This article proposes a novel method centered on oscillation rather than rotation, leveraging flux-induced oscillation for energy absorption. Although oscillation is typically considered detrimental to structures (Xu et al. 2019), it holds potential for energy extraction when thoroughly researched. Demonstrating practicality through scale models and prototypes (Bernitsas et al. 2008)), this oscillation-based approach minimizes environmental impact, especially in utilizing small waterfalls.

Introducing a turbine based on the torsional galloping effect with magnetic restoration (Padilha de Lima 2019) (Padilha de Lima 2021), this research pioneers the application of flow-induced oscillation for hydroelectric energy extraction from sources with minor heads. The study aims to conduct theoretical and numerical analyses to determine the most efficient turbine arrangement, advancing the understanding and implementation of sustainable energy solutions.

## 2 BIBLIOGRAPHIC REVIEW

### 2.1 Flow Induced Oscillation Rating

Based on where they come from, resonance or instability, flux-induced oscillations can be categorized into one of two groups (van Oudheusden 1992). If the frequency of the oscillatory forces matches the inherent frequency of the elastic structure, resonance oscillations occur. The oscillatory force that causes oscillations through resonance may result from the oscillation of the input flow, in which case the phenomena is referred to as buffeting, or from the shedding of vortex, in which case the phenomena is referred to as VIV. The oscillatory force that causes oscillations through instability may have two or more degrees of freedom, in which case the phenomena is known as flutter, or simply one de-

gree of freedom, in which case it is known as galloping (Fernandes et al. 2014). There are two variations of the galloping oscillation action. The torsional, which occurs when the body oscillates just while it is rotating, and the translational, which occurs when the body oscillates both spinning and translating.

### 2.2 Turbine Description

The turbine is composed of a flat plate or hydrodynamic profile, exposed to a steady current that induces torsional oscillations around its vertical axis. The proposed design incorporates four magnets, with two attached to the trailing edge of the turbine and the other two affixed to permanent supports, limiting rotor movement. Strategic magnet placement ensures mutual resistance between any two magnets on the same side of the turbine. Consequently, the turbine undergoes a magnetic restoration force when moved in either of its two potential orientations. This interplay between magnet configuration and magnetic restoration defines the turbine's functionality. The profile, featuring connected magnets, is depicted in the top view in Figure 1 a), highlighting the turbine's length parameters. The schematic top view of the system is presented in Figure 1 b), with a focus on the turbine configuration details.

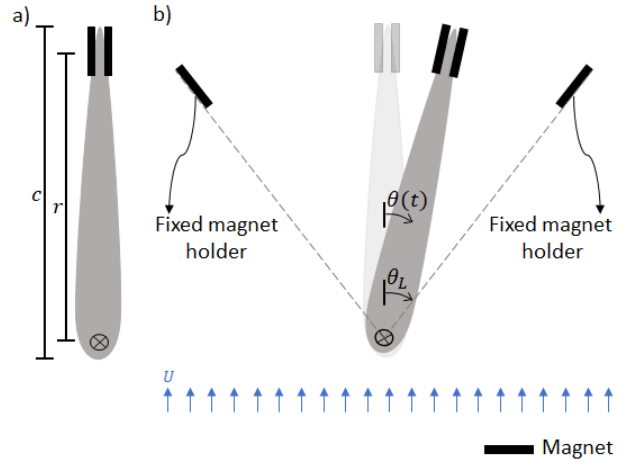


**Figure 1: Schematic top view of the turbine, with parameters definition.**

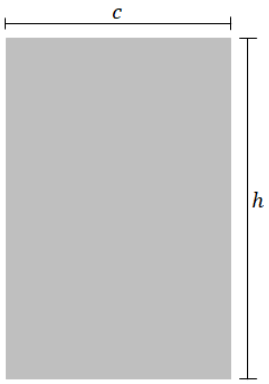


**Figure 2: Schematic front view of the turbine, with parameters definition.**

Figure 2 shows a schematic side view of the turbine, where we can see the definition of the chord ($c$) and height ($h$) parameters.

### 2.3 Scientific Gap

The low efficiency of a turbine relying on the torsional galloping effect, with restoration from linear and torsional springs, prompted the initiation of the study. The significant amplitudes of turbine movement were identified as a key factor contributing to the observed inefficiencies. The generation of substantial vortexes at both the leading and trailing edges of the turbine led to considerable energy dissipation. This loss of energy, which is not absorbed, results in diminished effectiveness (Fernandes et al. 2014). To address this issue and restrict the turbine's range of motion, thereby enhancing its efficiency, one proposed solution is the implementation of magnetic restoration.

In preparation for submitting a patent application for the devised technique, an exhaustive analysis of analogous turbines was conducted. This examination unveiled innovations outlined in patents such as (Villarreal 2015), (Lynch 2012), (Carney 2006), (KIOST 2017), and (Yoshihiko 2017). These patents detail oscillatory systems designed to harness energy from fluid flow, where the oscillation is induced by vortex phenomena (Vortex-Induced Vibration or VIV). Notably, these systems incorporate mechanical controls capable of adjusting damping, restoring force, and moment of inertia associated with the oscillatory motion. The method outlined in (Villarreal 2015) employs permanent magnets as part of this mechanical control mechanism.

The existing body of knowledge includes oscillatory systems designed to harness energy from fluid flow, with oscillations generated by flutter-type instabilities. Examples of such systems are the Stingray prototypes (Padilha de Lima 2019) (Padilha de Lima 2021) developed by Engineering Business Ltd. and the Pulse-Stream 100 (Padilha de Lima 2019) (Padilha de Lima 2021) by Pulse Tidal Ltd. These prototypes underwent field testing, revealing energy generation figures that were economically unfeasible. Moreover, the systems exhibited a complex mechanical structure necessary to sustain the oscillating profile and overall system integrity.

Notably, within the current state of the art, there are no instances of oscillatory systems utilizing fluid flow for energy generation and relying on permanent magnets to restore oscillation induced by instability of the galloping type. Hence, the subject of investigation in this article represents a novel contribution to the field.

**Table 1: Description of variables used.**

| Nomenclature | | | |
|---|---|---|---|
| $\theta(t)$ | Turbine instantaneous position angle $[rad]$ | $\nu$ | Kinematic viscosity $[m^2.s^{-1}]$ |
| $\dot{\theta}(t)$ | Turbine instantaneous angular velocity $[rad.s^{-1}]$ | $\omega$ | Response frequency $[rad.s^{-1}]$ |
| $\ddot{\theta}(t)$ | Turbine instantaneous angular acceleration $[rad.s^{-2}]$ | $U$ | Uniform current speed $[m.s^{-1}]$ |
| $K$ | Reduced frequency $[-]$ | $\theta_L$ | Positioning angle of fixed magnets $[rad]$ |
| $C(K)$ | Lift reduction factor $[-]$ | $k_M(t)$ | Magnetic restoration coefficient $[kg.m^2.s^{-1}]$ |
| $H_n^{(2)}(K)$ | Henkel function of the second kind $[-]$ | $k_H$ | Hydrodynamic restoration coefficient $[kg.m^2.s^{-1}]$ |
| $J_n(K)$ | Bassel function of the first kind $[-]$ | $b_H$ | Hydrodynamic damping coefficient $[kg.m^2.s^{-2}]$ |
| $Y_n(K)$ | Bassel function of the second kind $[-]$ | $\rho$ | Water density $[kg.m^3]$ |
| $I$ | Total moment of inertia $[kg.m^2]$ | $C_M$ | Magnetic proportionality constant $[kg.m^2.s^{-2}]$ |
| $I_S$ | Structural moment of inertia $[kg.m^2]$ | $J$ | Magnetic constant of magnets $[kg.m^3.s^{-2}]$ |
| $I_{66}$ | Added moment of inertia $[kg.m^2]$ | $r$ | Distance of the magnets to the turbine shaft $[m]$ |
| $C_b$ | Damping proportionality constant $[kg.m^2]$ | $h$ | Turbine height $[m]$ |
| $\zeta$ | Total damping factor $[-]$ | $c$ | Turbine total length (Turbine chord) $[m]$ |
| $\zeta_M$ | Mechanical damping factor (structural+hydrodynamic) $[-]$ | $Re$ | Reynolds number $[-]$ |
| $\zeta_{PTO}$ | Damping factor due to power take-off $[-]$ | $TSR$ | Tip Speed Ratio $[-]$ |
| $m$ | Turbine mass $[kg]$ | | |

## 3 METHOD

### 3.1 Mathematical Model

In Figure 3 we see the schematic top view of the turbine with the representation of the moments that act on it when it moves.

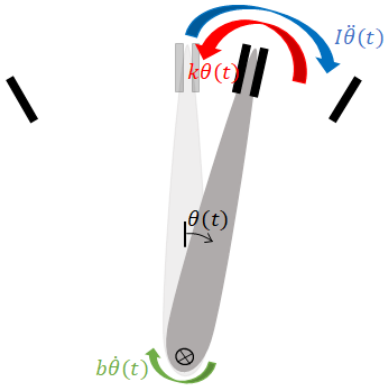


**Figure 3: Schematic front view of the turbine, with the moments acting on the turbine when it moves.**

The problem's selected mathematical model system is displayed in Equation 1 and Equation 2.

$$I\ddot{\theta}(t) + b\dot{\theta}(t) + k\theta(t) \tag{1}$$

Or:

$$I\ddot{\theta}(t) + \left(C_b\sqrt{(k_M(t) - k_H)\frac{1}{I}} + b_H\right)\dot{\theta}(t) + (k_M(t) - k_H)\,\theta(t) = 0 \tag{2}$$

The hydrodynamic restoring coefficient, $k_H$, and the hydrodynamic damping coefficient, $b_H$, solely result from the potential component of the flow around a flat plate and are derived through Theodorsen's potential theory (Theodorsen 1949). The computations for these coefficients are outlined in Equation 3 and Equation 4, respectively.

$$b_H = -\left(\frac{\pi\rho c^3 U h}{16}\right)(1 - 3C(K)) \tag{3}$$

$$k_H = \frac{3\pi\rho c^2 U^2 h C(K)}{4} \tag{4}$$

Here, $K$ represents the reduced frequency, computed using Equation 5, and $C(K)$ denotes the lift reduction factor, determined by Equation 6. The lift reduction factor, proposed by Theodorsen, quantifies the reduction in the lift force of a flat plate in percentage terms, attributed to the oscillation frequency ($\omega$).

$$K = \frac{\omega c}{2U} \tag{5}$$

$$C(K) = \left|\frac{H_1^{(2)}(K)}{H_2^{(2)}(K) + H_1^{(2)}(K)}\right| \tag{6}$$

Where $H_n^{(2)}(K)$ is the Hankel function of the second kind, calculated by Equation 7.

$$H_n^{(2)}(K) = J_n(K) - iY_n(K) \tag{7}$$

Where $J_n(K)$ is the Bassel function of the first kind, calculated by Equation 8, and $Y_n(K)$ is the Bassel function of the second kind, calculated by Equation 9.

$$J_n(K) = \frac{1}{2\pi}\int_{-\pi}^{\pi} e^{i(nr - Ksin(r))}dr \tag{8}$$

$$Y_n(K) = \frac{1}{\pi}\int_0^{\pi} sin\,(Ksin(r) - nr)\,dr - \frac{1}{\pi}\int_0^{\infty}\left(e^{nt} + (-1)^n e^{-nt}\right)e^{-Ksinh(t)}dt \tag{9}$$

The total moment of inertia, $I$, is calculated according to Equation 10.

$$I = I_S + I_{66} \tag{10}$$

Where the structural moment of inertia, $I_S$, is approximated as the moment of inertia of a flat plate. Equation 11 is used to calculate $I_S$.

$$I_S = \int_{Flatplate} x^2 dm = \frac{1}{12} mc^2 \tag{11}$$

And the added moment of inertia, $I_{66}$, is due to the potential portion of the flow around the flat plate and is calculated by Theodrosen (Theodorsen 1949) from Equation 12.

$$I_{66} = \frac{9\pi\rho c^4 h}{128} \tag{12}$$

The the damping proportionality constant, $C_b$, is calculated according to Equation 13.

$$C_b = 2I\zeta \tag{13}$$

The overall damping factor, $\zeta$, results from the combination of the mechanical damping factor, $\zeta_M$, and the power take-off damping factor, $\zeta_{PTO}$, as illustrated in Equation 14. The mechanical damping factor, $\zeta_M$, arises from the dissipation of energy by both the turbine structure and the fluid.

$$\zeta = \zeta_M + \zeta_{PTO} \tag{14}$$

The mathematical model delineated in Equation 1 exhibits non-linearity primarily attributed to the magnetic restoration segment. The magnetic restoration coefficient, $k_M$, undergoes non-linear variations contingent on the instantaneous turbine position, $\theta$, demonstrating symmetry at $\theta = 0$ and singular points at $\theta = \theta_L$ and $\theta = -\theta_L$, where $k_M$ tends toward positive infinity. This $k_M$ behavior contributes to turbine instability, visually evident in the continuous blue curve depicted in Figure 4. These curves were generated under the conditions of the turbine prototype, with $r = 0.2\ m$ and $J = 0.006901 N.m^2$ or $C_M = 0.0172525 N.m$, and $\theta_L = 30°$. The positions of the fixed magnets ($\theta_L$) are also denoted by vertical black lines in Figure 4.

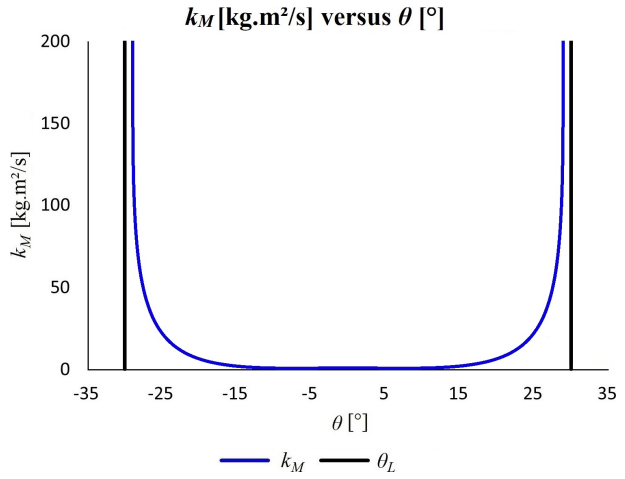


**Figure 4: $k_M$ curve as a function of $\theta$.**

Through an analytical examination of the issue, it becomes feasible to derive the equation for $k_M$ in terms of $\theta$ as illustrated in Equation 15. This computation is detailed in prior publications by the authors (Padilha de Lima 2019) (Padilha de Lima 2021).

$$k_M(\theta) = \frac{C_M}{\theta}\left(\frac{\cos\left(\frac{\theta_L-\theta}{2}\right)}{1-\cos(\theta_L-\theta)} - \frac{\cos\left(\frac{\theta_L+\theta}{2}\right)}{1-\cos(\theta_L+\theta)}\right) \tag{15}$$

The magnetic proportionality constant, $C_M$, is determined using Equation 16, where the magnetic constant of the magnets, $J$, is dependent on their composition and shapes, and the distance from the center of the magnets to the turbine axis, $r$.

$$C_M = \frac{J}{2r} \tag{16}$$

### 3.2 Numeric Solution

To derive the solutions $\theta(t)$ and $\dot{\theta}(t)$ for the nonlinear model, the 4th order Runge-Kutta method was employed on the nonlinear system described in Equation 1. The initial conditions for the Initial Value Problem (IVP) were set as $\theta(0) = \theta/2$ and $\dot{\theta}(0) = 0$. The method was executed over a time span of 120 seconds, discretized into 10000 points. Following the model solution and the acquisition of $\theta(t)$ and $\dot{\theta}(t)$, the available power ($P_A$) for the problem was computed using the relationship outlined in Equation 17 (Fernandes et al. 2014). This expression accounts for the energy of a flow with density $\rho$ and speed $U$ traversing through an area $A$.

$$P_A = \rho U^3 A \tag{17}$$

Since $A$ is the projected area of the turbine perpendicular to the flow, the value of $A$ is calculated from Equation 18.

$$A = hcsin(\theta_0) \tag{18}$$

Where $\theta_0$ is the amplitude of $\theta(t)$, obtained from the model solution. Therefore, $P_A$ can be calculated with Equation 19.

$$P_A = \rho U^3 hcsin(\theta_0) \tag{19}$$

The value of $\theta_0$ is determined based on the final 30 seconds of the 120 seconds solution. This 90 seconds interval is sufficient for the solution to either converge to a cyclic limit solution or to a stationary solution. In the case of convergence to a stationary solution, the amplitude value ($\theta_0$) becomes zero, resulting in a null available power ($P_A$). Following the model solution to obtain $\dot{\theta}(t)$, it becomes feasible to compute the power generated by the turbine, $P_{TO}$, utilizing the relationship outlined in Equation 20.

$$P_{TO} = \frac{1}{T}\int_0^T M_{PTO}(t)\dot{\theta}(t)dt \tag{20}$$

Where $M_{PTO}$ is the moment of energy absorption. As only the moment term, proportional to $\zeta_{PTO}$, performs energy absorption work, we have that the moment $M_{PTO}$ is given by Equation 21.

$$M_{PTO} = b_{PTO}\dot{\theta}(t) = 2\zeta_{PTO}\sqrt{Ik(t)}\dot{\theta}(t) \tag{21}$$

In this way, the power absorbed by the turbine, $P_{TO}$, is obtained by solving the Equation 22.

$$P_{TO} = \frac{1}{T}\int_0^T 2\zeta_{PTO}\sqrt{Ik(t)}\left(\dot{\theta}(t)\right)^2 dt \qquad (22)$$

The integral to obtain the absorbed power $P_{TO}$, is performed numerically by the trapezoidal method, also being calculated only for the last 30 seconds, time in which convergence has already occurred.

From the calculated powers, it is also possible to calculate the theoretical efficiency of the turbine, which is the ratio between the absorbed power, $P_{TO}$, by the available power, $P_A$. A flowchart for solving the non-linear model is shown in Figure 5.

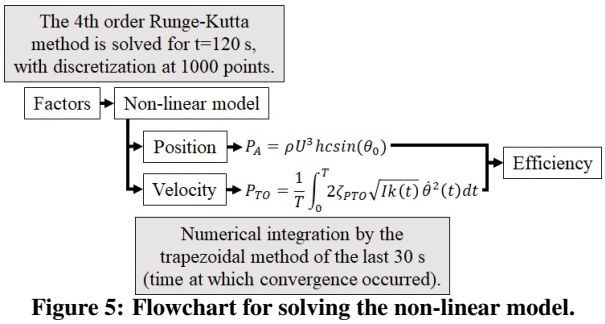


**Figure 5: Flowchart for solving the non-linear model.**

### 3.3 Analysis of Variance

To select the optimal variables for stability analysis, we performed a variance analysis. A dimensionless analysis was then conducted to obtain dimensionless variables that govern the problem, facilitating the variance analysis. The analytical variables selected for this purpose included $J$, $\theta$, $\theta L$, $U$, $h$, $c$, $m$, $\nu$, $\omega$, and $\zeta_{PTO}$.

Utilizing the stages of Buckingham's $\pi$ Theorem (Buckingham 1915), we conducted a dimensional analysis of the turbine issue, leading to the generation of dimensionless quantities as outlined in Equation 23.

$$\theta = f\left(\frac{J}{mcU^2}, \theta_L, \frac{h}{c}, Re = \frac{Uc}{\nu}, TSR = \frac{\omega c}{U}, \zeta_{PTO}\right) \qquad (23)$$

The comparison of means among two or more populations is examined through analysis of variance (ANOVA). These analyses assess the significance of one or more factors by contrasting means of response variables across different factor values. The null hypothesis posits that all population means (factor level means) are identical, while the alternative hypothesis suggests that at least one differs.

If the P-value, associated with the F-Value, is smaller than the alpha within its significance interval, it indicates that the factor's variance significantly influences the variable of interest, exerting a distinct effect on its mean compared to other means.

In this study, six out of the seven dimensionless components identified through dimensional analysis were chosen as factors. The dimensionless $TSR$ was excluded due to its lack of frequency dependence ($\omega$), a feature present in the model solution, disqualifying it as a factor.

A full factorial experiment was conducted with the six selected components, each with two levels, resulting in $2^5 = 64$ tests. Values resembling those found in the LOC were chosen for the factor levels. Table 2 presents the values of the selected levels.

**Table 2: Chosen values for factor levels.**

| Factor | Type | Levels | Values |
|---|---|---|---|
| $J/(mcU^2)$ | Fixed | 2 | 0.04, 0.05 |
| $\theta_L$ | Fixed | 2 | 25, 35 |
| $a/c$ | Fixed | 2 | 0.5, 2.5 |
| $Re$ | Fixed | 2 | 100000, 200000 |
| $\zeta_{PTO}$ | Fixed | 2 | 0.2, 0.5 |

## 4 RESULTS AND DISCUSSION

### 4.1 Analysis of Variance

The solution to the nonlinear system was obtained, and the theoretical efficiency for each of the 64 planned trials was determined.

The outcomes of this analysis for each variable are presented in Table 3.

**Table 3: Result of analysis of variance.**

| Factor | GL | SQ (Aj.) | QM (Aj.) | F-Value | P-Value |
|---|---|---|---|---|---|
| $J/(mcU^2)$ | 1 | 0.00000 | 0.00000 | 0.00 | 1.000 |
| $\theta_L$ | 1 | 0.23602 | 0.23602 | 6.63 | 0.013 |
| $h/c$ | 1 | 0.06296 | 0.06296 | 1.77 | 0.019 |
| $Re$ | 1 | 0.93481 | 0.93481 | 26.25 | 0.000 |
| $\zeta_{PTO}$ | 1 | 3.02183 | 3.02183 | 84.87 | 0.000 |
| Error | 57 | 2.02957 | 0.03561 | | |
| Total | 63 | 6.33514 | | | |

With a confidence level of 95%, we can dismiss the impact of factors on the model when their P-Value exceeds 0.05. Consequently, at a 95% significance level, the factor $J/(mcU^2)$ does not influence efficiency. The impact of factors on efficiency is illustrated in Table 4.

**Table 4: Influence of factors for efficiency.**

| Factor | Influence on efficiency [%] |
|---|---|
| $\zeta_{PTO}$ | 70.1 |
| $Re$ | 19.2 |
| $\theta_L$ | 5.1 |
| $h/c$ | 4.8 |
| $J/(mcU^2)$ | 0.2 |

As per the analysis of variance, the parameters exerting the most significant influence on efficiency are $\zeta_{PTO}$ (70.1%), $Re$ (19.2%), $\theta/L$ (5.1%), and $h/c$ (4.8%). The other components exhibit minimal impact on efficiency. A crucial implication of this observation is that, for scale tests, ensuring equality among the components with the greatest influence on the model ($\zeta_{PTO}$, $Re$, $\theta/L$, and $a/c$) is adequate.

### 4.2 Numeric Solution

In the numerical exploration, varying $\theta_L$ values of 15°, 20°, 25°, 30°, 35°, 40° and 45° and $\zeta_{PTO}$ values of 0.05 to 0.9 with an increment of 0.05 were selected. The corresponding $Re$, $h/c$ and $\zeta_{PTO}$ values were adjusted for each angle, and the theoretical efficiency for each point was calculated. These efficiencies are then depicted on a graph.

The $Re$ values span from 0 to 45 $\times 10^4$ with an increment of 9000, resulting in a total of 51 values. For $h/c$, the values range from 0 to 3, with an increment of 0.06, totaling 51 values. Consequently, the model is evaluated for 51 × 51 = 2601 scenarios for each efficiency graph. To reduce computational time, the strategy involved a reduction in the number of points. The investigated $Re$ values are constrained within the limits applicable in the LOC, defined by a turbine chord of 1.5 m and a maximum current velocity of 0.5 $m/s$. The efficiency diagrams for $\zeta_{PTO} = 0.40$, $\zeta_{PTO} = 0.45$ and $\zeta_{PTO} = 0.50$ are depicted in Figure 6. To streamline the presentation of data, only the most crucial graphs for $\theta_L$ values of 25°, 30°, and 35° will be showcased. This is the result for the first phase of project optimization.

In the second phase, the turbine configuration with the best efficiency is sought in a smaller range of parameters. For this, the $\zeta_{PTO}$ and $\theta_L$ values where the highest efficiencies were found are selected and the $Re$ and $h/c$ values are varied. By selecting the value of $\theta_L = 0.45$ and $\theta_L = 30°$, the studied $Re$ values will be from 20 $\times 10^4$ to 25 $\times 10^4$ with a step of 1000, resulting in a total of 51 values, and the values of $h/c$ from 1.25 to 1.75 with a step of 0.01, resulting in a total of 51 values. This efficiency diagram is presented in Figure 7. This is the result for the second phase of project optimization.

The maximum efficiency found for the system is 57%, for the condition with $\theta_L = 30°$, $\zeta_{PTO} = 0.45$, $h/c = 1.57$ and $Re$ = 23.6 × $10^4$.

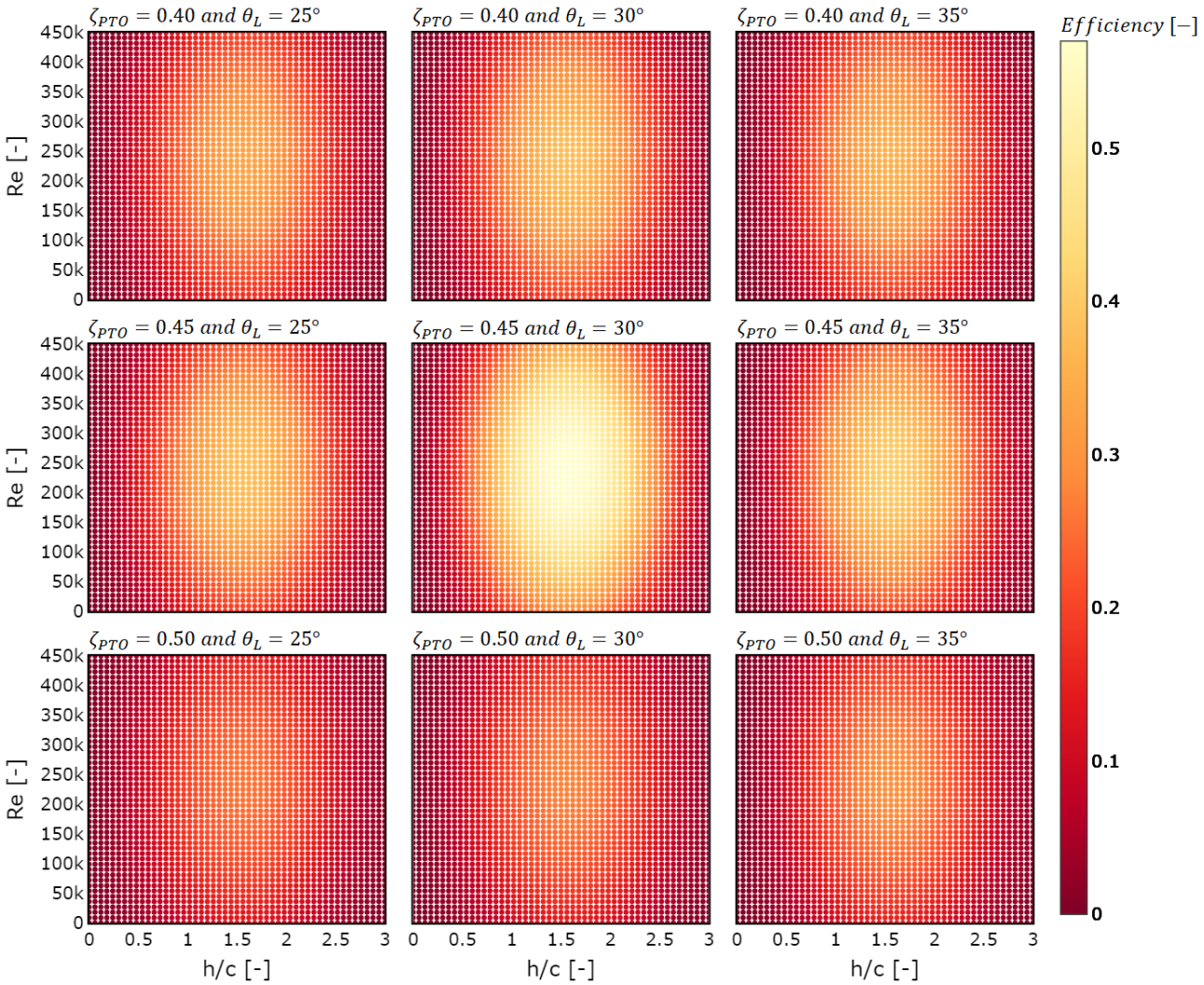


**Figure 6: Efficiency diagrams for $\zeta_{PTO} = 0.40$, $\zeta_{PTO} = 0.45$ and $\zeta_{PTO} = 0.50$ with $\theta_L = 25°, 30°$ and $35°$.**

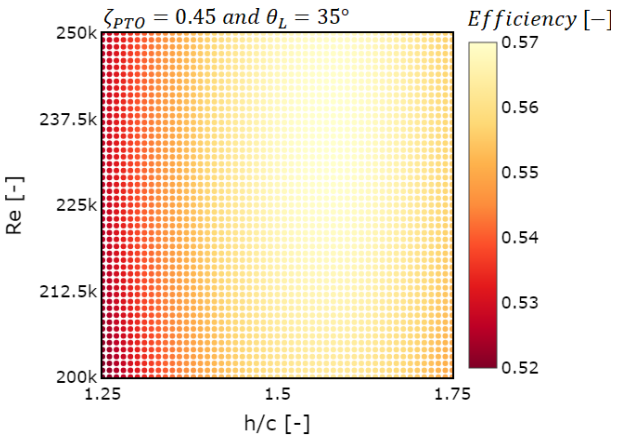


**Figure 7: Efficiency diagram for $\zeta_{PTO} = 0.45$ and $\theta_L = 30°$.**

## 5 CONCLUSIONS

The identification of the optimal turbine efficiency condition was successfully accomplished. This involved considering the damping factor arising from the absorption of energy that the generator must fulfill. The system's maximum efficiency was determined to be 57%, observed under the condition with $\theta_L = 30°$, $\zeta_{PTO} = 0.45$, $a/c = 0.25$, and $Re = 15 \times 10^4$. This efficiency corresponds to $57\%/59.3\% = 96.2\%$ of the maximum achievable value, as indicated by Betz (Betz 1966).

## 6 ACKNOWLEDGMENTS

This work was financed in part by the Coordenação de Aperfeiçoamento de Pessoal de Nível Superior – Brasil (CAPES) – Finance Code 001". The CNPq (Brazilian National Research Council) is also greatly acknowledged.

The authors would like to also acknowledge the assistance of Laboratory of Waves and Currents (LOC/COPPE-UFRJ) and Institute for Fluid Dynamics and Ship Theory (FDS-TUHH).

## REFERENCES

Bagher, A. M., Vahid, M., Mohsen, M., and Parvin, D. (2015). Hydroelectric energy advantages and disadvantages. American Journal of Energy Science, 2(2):17–20.

Bernitsas, M. M., Raghavan, K., Ben-Simon, Y., and Garcia, E. M. H. (2008). VIVACE (vortex induced vibration aquatic clean energy): A new concept in generation of clean and renewable energy from fluid flow. Journal of Offshore Mechanics and Arctic Engineering, 130(4).

Betz, A. (1966). Copyright. In Introduction to the Theory of Flow Machines, page 4. Pergamon.

Buckingham, E. (1915). The principle of similitude. Nature, 96(2406):396–397.

Carney, M. E. (2006). Energy capture in flowing fluids. Patent US20080048455A1.

Dametew, A. W. (2016). Design and analysis of small hydro power for rural electrification. Global Journals of Research in Engineering, 16(F6):25–45.

Elavarasan, R. M. (2019). The motivation for renewable energy and its comparison with other energy sources: A review. European Journal of Sustainable Development Research, 3(1).

Erlach, J. (1889). Pelton turbine. Patent US4950130A.

EU (2019). Paris agreement. The European Green Deal.

Fernandes, A. C. and Armandei, M. (2014). Low-head hydropower extraction based on torsional galloping. Renewable Energy, 69:447–452.

Hood, E. K. (1910). Propeller turbine. Patent US975526A.

KIOST, K. I. o. O. S. T. (2017). Vortex induced vibration in generated oscillation plant by support. Patent KR101309126B1.

Padilha de Lima, J. V. (2019). Innovative turbine based on torsional galloping with magnetic magnetic.Course completion work at UFRJ.

Padilha de Lima, J. V. (2021). Innovative current turbine based on directional instability and magnetic restoration. Master's thesis at UFRJ.

Loney, M. (1995). Social problems, community trauma and hydro project impacts. Canadian Journal of Native Studies, 15(2):231–254.

Lynch, G. J. (2012). Adaptive hydrokinetic energy harvesting system. Patent US9006919B2.

Naskali, P. H., MacLean, A., C. C. Gray, Neil; Lewis, J. H., and Newall, A. P. (2005). Helical turbine. Patent US7344353B2.

Noel, P. R. (1967). Axial flow rotor turbine. Patent US3389889A.

ONU (1998). Kyoto protocol to the united nations framework convention on climate change. United Nations.

ONU (2015). Paris agreement. United Nations.

Peng, Z. and Zhu, Q. (2009). Energy harvesting through flow-induced oscillations of a foil. Physics of Fluids, 21(12):123602.

Rahman, A., Farrok, O., and Haque, M. M. (2022). Environmental impact of renewable energy source based electrical power plants: Solar, wind, hydroelectric, biomass, geothermal, tidal, ocean, and osmotic. Renewable and Sustainable Energy Reviews, 161:112279.

Sproule, R. S. (1961). Kaplan turbine. Patent US3146990A.

Theodorsen, T. (1949). General theory of aerodynamic instability and the mechanism of flutter. Work of the US Gov. Public Use Permitted.

van Oudheusden, B. (1992). Investigations of an aeroelastic oscillator: Analysis of one-degree-of-freedom galloping with combined translational and torsional effects. Delft University of Technology.

Villarreal, D. J. Y. (2015). Electric power generator and a method of generating power electricity. Patent US10641243B2.

Williams, H. L. (2006). Open center fan turbine.

Patent USD543495S1.

Xu, Z.-D., Chen, Z.-H., Huang, X.-H., Zhou, C.-Y., Hu, Z.-W., Yang, Q.-H., and Gai, P.-P. (2019). Recent advances in multi-dimensional vibration mitigation materials and devices. Frontiers in Materials, 6:143.

Yasuyuki, E., Kaneo, S., and Sadao, K. (2004). Francis turbine. Patent US7128534B2.

Yoshihiko, H. (2017). Bistable non-linear pendulum generator using fluid. Patent JP6001732B1.

Zhou, J.-L., Zhe-Hua, B., and Sun, Z.-Y. (2013). Safety assessment of high-risk operations in hydroelectricproject based on accidents analysis, sem, and anp. Mathematical Problems in Engineering, 2013.